# MATERIAL SCIENCE OF Nb RF ACCELERATOR CAVITIES: WHERE DO WE STAND 2001?

J. Halbritter
Forschungszentrum Karlsruhe, Institut für Materialforschung I
Postfach 3640, 76021 Karlsruhe , Germany

*Abstract*

The rf losses, especially actual level and increase with rf fields, limit most stringently the application of superconducting rf cavities. This is due to the needed cooling power to be supplied locally to the high field region causing rf breakdown. The rf losses are due to two sources based on different physics: dielectric rf losses proportional to $R^E E^{\perp 2}$ and shielding current losses proportional to $R^H H^{\parallel 2}$. Material science wise intrinsic losses $R_{BCS}$ are separate from extrinsic, rf residual losses $R_{res}$. The separation of $R_{res}(T,f,H)$ from the BCS losses $R_{BCS}(T,f,H)$ yields the quasi-exponential increases of the electric surface resistance with the electric field $E^{\perp}$ perpendicular to the surface $\delta R^E(E^{\perp}) \propto \exp(-c/E^{\perp})$ and the power law increases of the magnetic surface impedances with the magnetic field $H^{\parallel}$ parallel to the surface $\delta R^H(H^{\parallel}) \propto (H^{\parallel})^{2n}$ (n = 1, 2. .). By $Nb/Nb_2O_{5-y}$ interfaces of external and internal surfaces $R^H_{res}(T,f)$ and $R^E_{res}(f,E^{\perp})$ can be explained quantitatively by localized states $n_L$ of $Nb_2O_{5-y}$ in close exchange with extended states $n_m$ of Nb. Especially, the Q-drop $\propto 1/R^E(E^{\perp})$ and its reduction by EP- and BCP-smoothening and by UHV anneal at T≈100°C are well accounted for by interface tunnel exchange. The UHV anneal not only reduces surface scattering and $R^E$ but also enforces the $R_{BCS}$(T, 1.3 GHz, H < 10 mT)-drop and reduces $R_{BCS}$(T, ≈ GHz, ≈ 10 mT) by more than a factor 2. The interrelations $R_{BCS}$-drop, $R^E$ and $R_{BCS}$ with the material science of $Nb_2O_{5-y}$/Nb interfaces, e.g., by EP or UHV anneal, will be elucidated.

## 1 INTRODUCTION

The technology to produce Nb rf accelerator cavities with gradients above $E_{acc} \approx 10$ MeV/m and $Q_o$ (2K; 1 GHz) $\approx 10^{10}$ is now in hand and delivered by industry, as the result of more than 30 years intensive research and developments started first at Stanford [1] and Karlsruhe [2]. But still progress is needed to fulfill the ever growing desire of, e.g., the high energy physics community [3]. Highlights in the recent progress are discussed below. Progress usually starts with a name, like Q-decease or Q-drop, followed by quantification and then the decease can be overcome. The progress to be reported in Nb cavitiy performance is based on basic research carried through by groups at CEBAF, DESY, INFM, KEK and SACLAY, discussed in Sects. 4 and 5.

Where stands the materials science of superconducting Nb rf cavities and surfaces at the moment? Firstly, Nb free of inclusions, like big Ta- or $NbO_x$-lumps, with a dc resistance ratio RRR > 200 is now available [3]. Secondly, high pressure (80 bar) water rinsing (HPR) [4] is able to reduce the dust on Nb surfaces sufficiently. Thirdly, we are left with intrinsic Nb corrosion yielding after electropolishing (EP) or buffered chemical polishing (BCP), followed in both cases by HPR, some inhomogeneities, as sketched in Fig. 1.

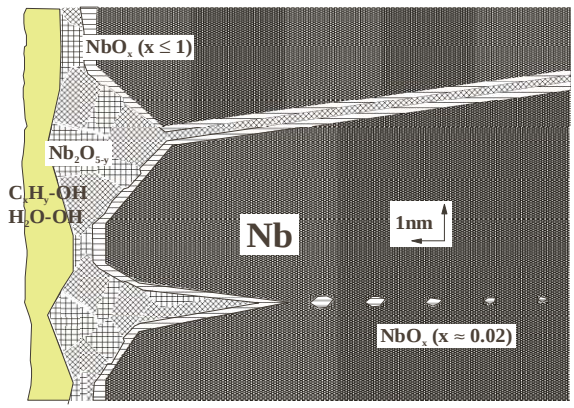


**Fig. 1:** Nb surface with crack corrosion by oxidation by $Nb_2O_5$ volume expansion (factor 3). $Nb_2O_{5-y}$-$NbO_x$ weak links/segregates (y, x < 1) extend up to depths between 0.01 – 1/ 1-10 μm for good – bad Nb quality and weak - strong oxidation [8]. Embedded in the adsorbate layer of $H_2O/C_xH_yOH$ (≥ 2 nm) being chemisorbed by hydrogen bonds to $NbO_x(OH)_y$, adsorbate covered dust is found. This dust yields enhanced field emission (EFE [7]) summarized in Sect. 3.1.

Crucial are the scales: Nb is coated by less than 0.5 nm $NbO_x(x \leq 1)$ and by 1 – 3 nm $Nb_2O_{5-y}$ covered with hydrogen bonded $H_2O/C_xH_y$ $(OH)_z$ of similar thickness. Optimal superconducting Nb properties have to hold, at least, in a penetration depth $\lambda^H(T<T_c/2) \approx 40$ nm. Another scale is the dimension of Cooper pairs $\xi_F \approx 60$ nm, where metallic defects in Nb have to be much smaller in size to sustain overall good Nb properties. Similarly on $Nb_2O_5$, dust and protrusions have to be reduced in amount and size to get good electric field properties. This needed homogeneity in and on Nb is achieved now yielding $E_{acc} \geq$ 30 MeV/m The scales of 1 - 10 nm for Nb cleanliness and homogeneity have to be compared to accelerator lengths of 0.1 -1 km, showing a reproducibility over 10 order in magnitude being now achieved. This, by itself, is a big achievement. But as we see from semiconductor industry, there is still more to come. As material scientist, I will not dwell on this but I want to outline old and new Nb results and understandings, where, in my view, progress, has been made in the last years and will be made in the next years.

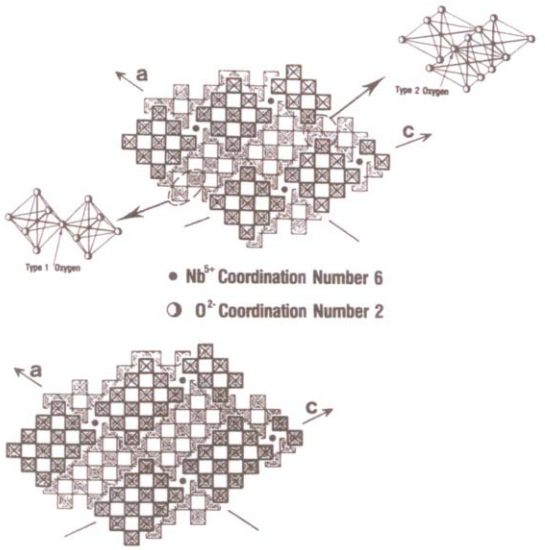


**Fig. 2:** $Nb_2O_{5-y}$ drawn as idealized octahedra, where the black circles are Nb atoms in tetragonal positions and outline the unit cell in projection, with octahedra sharing corners (Type 1 O) and sides (Type 2 O) yielding crystallographic shear planes where O-vacancies occur most easily, as insert Top: $Nb_2O_5$: The lighter form the 2 – 5 blocks at one level, the heavier forms are the 3 x 4 blocks at the second level. The levels are connected via corner sharing octahedra and via side sharing octahedra. Adjacent to the planes of side sharing octahedra are the crystallographic shear planes. Bottom: $Nb_{22}O_{54}$: The octahedra form 3 x 3 and 3 x 4 blocks at the second level with one O-vacancy at a shear plane.

## 2 CHEMISTRY AND MORPHOLOGY OF THE Nb-$Nb_2O_5$-ADSORBATE SYSTEM

In Fig. 1 a typical surface is shown being homogenized and cleaned by heating in UHV or in a Ti-enclosure above 1000 – 1400°C followed by BCP or EP and HPR [3,4]. Starting from the vacuum side, by its strong hydrogen bonds the NbOOH surface is coated by 2 – 10 monolayers (ML) of $H_2O$ and hydrocarbons [5-7], where the last 2 ML cannot be removed by UHV annealing below about 300°C. Embedded in this soup, dust coated by water and hydrocarbons may cause surface flashover and enhanced field or secondary electron emission [7]. Dust has been reduced drastically by intense HPR making so surface field strengths above 10 MV/m possible [3,4]. By the high energy per bond of 7 eV in the metallic interface oxide $NbO_x$ ($x \approx 1$) and of 5 eV in the dielectric $Nb_2O_5$, any Nb surface gets oxidized instantaneously at pressures above $10^{-10}$ Torr below about $10^3$ K to thicknesses up to 1 – 3 nm $Nb_2O_5$ by the Cabrera-Mott process [8]. There $O^{2-}$ is driven by the potential through the $Nb_2O_{5-y}$ oxidizing the metallic $NbO_x$ to $Nb_2O_{5-y}$, therewith the Nb surface is strained yielding cracks and the $Nb_2O_{5-y}$ interface layers is compressed shifting all clumsy ions ($PO^+_2$, . . . ) out of the interface as known from the compact part of the double layer at metal-electrolyte interfaces. $Nb_2O_{5-y}$ is nanocrystalline by its edge connected NbO-octahedra blocks corresponding the valence 6, which in turn get side connected via crystallographic shear planes shown in Fig. 2 to achieve the proper valence 5 [8]. At shear planes oxygen vacancies occur easily yielding for 300 K surface oxides $n_L \leq 10^{19}/cm^3$ localized states at $E_F$, which tunnel along those shear planes with $\phi \approx 0.1$ eV as barrier height [8]. The states $n_L(z < 2$ nm) are in fast ($< 10^{-10}$sec) interface tunnel exchange (ITE) with Nb conduction electrons of density $n_m$ as sketched in Fig. 3 and summarized in Sect. 3.2.

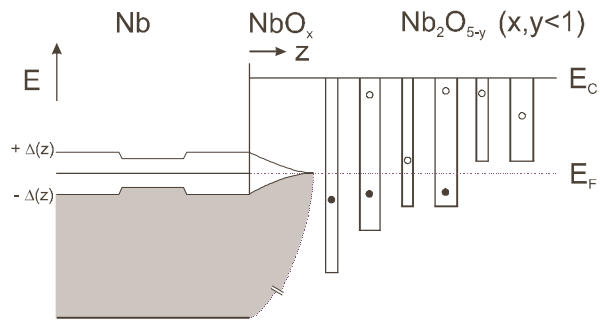


**Fig. 3:** Band structure at Nb-$NbO_x$-$Nb_2O_{5-y}$ interfaces with $E_c$-$E_F = \phi \approx 0.1 – 1$ eV as barrier heights for tunneling along crystallographic shear planes (~ 0.1 eV) or of $Nb_2O_{5-y}$ crystallites (~ 1 eV). Added is the superconducting energy gap $\Delta^*(z) < \Delta_o$ being reduced in $NbO_x$ clusters or interfaces and being normal conducting $\Delta^*$ ($z_L \geq 0.5$ nm) in localized states of $Nb_2O_{5-y}$. By their volume expansion those clusters locally enhance T* and $\Delta^* > \Delta_o$ in adjacent Nb by the uniaxal strain yielding a smeared BCS DOS.

For the conduction electrons ITE yields inelastic surface scattering described by a surface mean free path $l_s$ whereas the actual exchange with $Nb_2O_{5-y}$-states under influence of an rf electric field $E^{\perp}(t)$ correspond to dielectric interface losses $R^E$. According to [5,6] two major types of $Nb_2O_{5-y}$ coatings exists:

- fast, electrochemically grown wet oxide, e.g., by EP, of above 2 nm thick $Nb_2O_{5-y}$, coated by 5 – 10 ML water and hydrocarbons, with a high density of $n_L$ and with a cracked Nb surface [8]. The crack density and the size of $NbO_x$( $x < 0.2$)-precipitates and the amount and lengths of $Nb_2O_{5-y}$ filled weak links are enforced by strain and defects inside the Nb.
- dry oxidation yields thinner (< 2 nm), more uniform $Nb_2O_{5-y}$ coatings with only 2 – 3 ML water and hydrocarbons on top, with reduced charging, reduced ITE, reduced secondary emission [7] and reduced cracking [5,6,8].

The unperturbed bulk Nb has a $T_c = 9.25$ K and an average energy gap $\Delta_o(0) = 1.56$ meV, where 2 At % O degrades $T_c$ down to 7 K and $\Delta_o$ down by 20 to 30 %. The 2 – 3 ML thick metallic $NbO_x$($x \approx 1$) - layer between $Nb_2O_{5-y}$ and Nb has a reduced energy gap $\Delta^* < \Delta_o$. Inside the Nb below 600 K $Nb_2O_{5-y}$-weak links or $NbO_x$ ($0.2 \geq x \geq 0.02$) precipitate (Fig. 1) out of the Nb-O lattice gas [8]. By the enhanced volume of $NbO_x$-precipitates and of $Nb_2O_{5-y}$-interfaces the surrounding Nb lattice is compressed enhancing $\Delta^* > \Delta_o$ by up to 10 %, whereas at $NbO_x$ $\Delta^* < \Delta_o$ is depressed by 10 to 20 % [8]. The

intermingled enhanced and depressed $\Delta^*$ regions of sizes below about 5 nm « $\xi_F$ smear the BCS density of states and depress the average energy gap $\Delta < \Delta_o$.

Like the Nb-O-system below 600 K, picked up hydrogen precipitates to Nb-H below about 130 K preferably to form weak links nucleating close to the surface because of the NbH volume expansion [8,9]. $NbH_x$-precipitates are removed to larger depth by lattice compression by $NbO_x$-precipitates in the surface layer. Better is UHV anneal above 800°C, where $H_2$ is evaporated, and then sealing the surface by $Nb_2O_{5-y}$ to prevent H-pick-up.

## 3 INTERACTION OF RF-FIELDS WITH Nb CAVITY SURFACES

The rf fields at metallic surfaces can be separated in a rotational free component rot $\mathbf{E} \equiv 0$, namely $E^{\perp}$ giving rise to an electric field surface impedance $Z^E = R^E - i\omega\mu_o\lambda^E$ and in a divergence free component div $\mathbf{E} \equiv 0$, namely $H^{||}$ giving rise to rf shielding currents and a magnetic surface impedance $Z^H = R^H + i\omega\lambda^H$. Whereas the dielectric surface impedance $Z^E$ of clean metals is negligible because of $\lambda^E \leq 0.1$ nm [10], Nb-$Nb_2O_{5-y}$ by ITE cause a measurable $Z^E$ being discussed in Sect 3.2. By a penetration depth $\lambda^H(T < T_c/2, f < 100\ \text{GHz}) \geq 40$ nm and $\lambda^H(T > T_c) > \mu m/\sqrt{f/\text{GHz}}$ the shielding currents cause the dominant impedance $Z^H$ in superconducting and normal conducting rf cavities, the first being summarized below.

### *3.1 Electron loading*

The $E^{\perp}$-component causes electron emission where the gained energy of $e^-$ in the electric field then impinging on dielectric interfaces can cause enhanced electron emission, e.g. via secondary emission, via plasma generation [7] or via solid state double layers [11] enhancing the field emission directly or indirectly, described by the field enhancement factor $\beta$. HPR [3,4] has proven to be the adequate method to reduce dust and, hence, to reduce $\beta$ to values 100 yielding now $E_{acc} > 10$ MeV/m regularly.

### *3.2 Electric surface impedance $Z^E$ by ITE*

Whereas the intrinsic $Z^E$ of metals is negligible small [10,12b], the localized states $n_L$ of $Nb_2O_{5-y}$, at the Fermi energy $E_F$ (Fig. 3) by interface tunnel exchange (ITE) with the high DOS of Nb $n_m(E_F)$ enhances $Z^E$ by several orders of magnitude. Quantitatively, the exchange is governed by a tunnel rate (Fig. 3)

$$1/\tau(z_L,\varepsilon) = 1/\tau(0,\varepsilon)\exp(-2\kappa z_L)$$
$$\text{with } \kappa = \sqrt{2m(E_c - E_F)}/\hbar = \sqrt{2m\phi}/\hbar \qquad (1.1)$$

with $n_m \propto 1/\tau(0,\varepsilon)$. This exchange defines a distance $z^*(\omega)$ up to which the localized states are in equilibrium with the DOS of the metal for a rf field: $\omega\tau(z^*) = 1 = \omega\tau(0)\exp 2z^*(\omega)\cdot\kappa$. With the mean value $y^{-1}_n = z n_L(z)\, e^2/\varepsilon$ one obtains in the normal state:

$$\lambda^E_N = -z^*(\omega)^2/2y_n;$$
$$R^E_N = \frac{\omega\mu_o}{4\kappa^2}/2y_n\,(1-e^{-2\kappa z^*(\omega)}) \qquad (1.2)$$

According to Eqs. (1), $Z^E$ is proportional to $z^* n_L(z^*)$, i.e. linearly increasing with $n_L$ and exponentially with lowered barrier height $\phi$. The latter is quite small in $Nb_2O_{5-y}$ for crystallographic shear planes with $\phi \approx 0.1$ eV which house also the localized states $n_L \approx 10^{19}/\text{cm}^3$ [8,10b]. For normal conducting Nb estimates gave with $\varepsilon = \varepsilon_r\varepsilon_o$ and $\varepsilon_r(Nb_2O_{5-y}) \approx 10 - 15$ at the interface [10, 12b] $z^* \approx 1$ nm and

$$R^E_N(Nb - Nb_2O_{5-y}) \approx 10^{-4}\,\Omega/\varepsilon_r^2 \approx 10^{-6} - 10^{-7}\,\Omega \qquad (2.1)$$

at about 1 GHz. In the superconducting state an energy gap $|\varepsilon| < \Delta$ opens in $n_m(\varepsilon)$ blocking ITE. But for fields higher than $e z_E \beta^* E_{rf}/\varepsilon_r = \Delta$ ITE sets in where with the static, geometric field enhancement factor $\beta^* < 10$ the dielectric shielding $E^{\perp}\varepsilon_r = \beta^* E_{rf}$ overcomes the energy gap $\Delta$. $\beta^*$ is smaller than $\beta \approx 10^2 - 10^3$ being the dynamic field enhancement factor [7]. With Eq. (1.2) the high field $Z^E$ writes:

$$R^E_{res} = \frac{\omega\mu_o}{\kappa^2 4}\,\frac{1}{2y_n}(e^{-2\kappa z_E} - e^{-2\kappa z^*}) \qquad (2.2)$$

i.e. only states between $z_E$ and $z^*(\omega)$ cause ITE rf losses. Hence $R^E_{res}$ shows an onset at $E^\circ_{rf}$ increasing exponentially like $\exp(-2\kappa\Delta\varepsilon_r/e\beta^* E^{\perp})$ with $E^{\perp}$ till $R^E_{res}(E^{\perp})$ saturates when all states $n_L$ between $\{0, \min[z^*, d_{oxide}]\}$ participate in ITE, i.e. $R^E_{res}$ decreases with oxide thickness $d_{oxide} < z^*$. The small exponent $\Delta/\beta^*$ in Eq. (2.2) is fitted by a power series $E^{\perp n}$ starting with $4 \leq n \leq 16$ with n increasing by surface smoothness and reduced $n_L$ [10]. ITE in Eq. (2.2) develops out of standard field emission [7] by substituting $\phi = E_c - E_F \approx$ eV and $\beta \geq 10^2$ by $\Delta \approx$ meV and $\beta^* \ll \beta$ yielding as ratio between FE- and ITE- exponents $\phi/\Delta \approx 10^3$ due to resonant tunneling via intermediate states.

### *3.3 Intrinsic magnetic surface impedance $Z^H$*

The BCS-theory [12] is an excellent tool to obtain Nb material parameters as shown in [8] or Fig. 4 with agreement experiment/theory above 6 orders in magnitude in R(T). The parameters describing $Z^H$ of Nb are: the London penetration depth $\lambda_L(T=0) = 32$ nm, the dimension of Cooperpairs $\xi_F = 60$ nm and a mean free path l, the latter with its upper limit $l_s \sim \lambda_L/\sin 30° \approx 3\,\lambda_L$ by inelastic surface scattering via ITE by $Nb_2O_{5-y}$ [10] by trajectories with $\theta \approx 30°$ relative to the surface enhancing with $1/l = 1l/l_o + 1/l_s$

$$\lambda^H(T,l) \approx \lambda_L(T) f(\gamma)\sqrt{1+\xi_F/l} \quad \text{with } \gamma = \lambda_L/\xi_F \qquad (3)$$

with $f(\gamma) \sim 1/\gamma^{1/3}$ for $\gamma < 0.1$ by non-local effects [12a]. $\lambda^H(T) > \lambda_L(T)$ is only weakly depending on temperature below $T_c/2$, whereas above $T_c/2$ strong and preparation dependent $\lambda^H(T)$ increases have been reported [8].

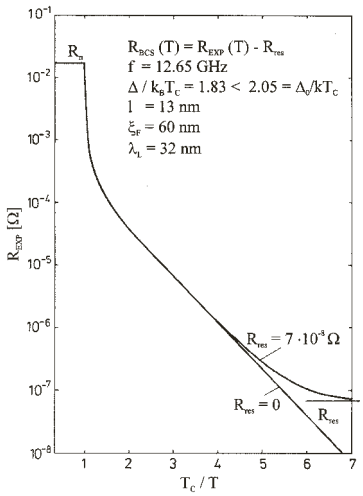


**Fig. 4:** Surface resistance an function of temperature T at 12.6 GHz of RRR = 30 Nb.

Especially the $\lambda^H(T^*_c)$ jump being related to stretches of $NbO_{0.02}$-clusters with $T^*_c \approx$ 6-7 K are worth mentioning [8] being indicated in Fig. 1.

In contrast to $\lambda^H(T \le T_c/2,\ \hbar\omega < \Delta/10) \approx$ const., the surface resistance $R^H(T,f,H)$ has been studied intensively in the last years because of its direct relevance to superconducting rf accelerator performance [3]. The surface resistance in the BCS theory needs a complex computer code, hence in the following the relevant dependencies for Nb-material science are made obvious only:

$$R(T,f) \approx c(\hbar\omega) \int_{\Delta}^{\infty} d\varepsilon 2[f(\varepsilon) - f(\varepsilon+\hbar\omega)] \cdot N(\varepsilon)N(\varepsilon+\hbar\omega) \cdot \int d^3k\ d^2p_i\ d^2p_f\ |<p_i \mid A(k) \mid p_f>|^2 / H^{\|2} \quad (4.1)$$

with $f(\varepsilon) = 1/(\exp(\varepsilon/kT) + 1)$ the Fermi function, with the density of states $N(\varepsilon) \approx (|\varepsilon|)/\sqrt{\varepsilon^2 - \Delta^2}$ with the BCS gap of $2\Delta$, with A(k) the photon momenta $k = k^{\perp}$ available for absorption with rot $\mathbf{A} = \mathbf{H}$ and $\mathbf{p}_i$ (initial) and $\mathbf{p}_i$ (final) momenta of the quasiparticles absorbing the photons ($\hbar\mathbf{k}$, $\hbar\omega$) in dipole approximation. In Fig. 5 the normalized absorption rate of photons is plotted versus $\hbar\omega/2\Delta$ with $\gamma$ as parameter. Obvious is the strong dependence of the photon absorption rate $r = R/\lambda_L\hbar\omega$ on $\gamma$, in clear contradistinction to any two fluid model. Also the frequency dependence deviates form $R \propto \omega^2$, i.e. $r \propto \omega$, in the direction of $R \propto \omega^{3/2}$ which is due to the BCS singularities in $\int_{\Delta}^{\infty} d\varepsilon N(\varepsilon)N(\varepsilon+\hbar\omega)$ in Eq. (4.1) [12] yielding:

$$R_{BCS}(T,\omega) \approx c\,\omega^2 N(\Delta+\hbar\omega)\left[f(\Delta) - f(\Delta+\hbar\omega)\right]M^2 \approx c^*\omega^2\Delta/kT\sqrt{2\hbar\omega\Delta}\ \exp(-\Delta/kT) \quad (T \le T_c/2, \hbar\omega << \Delta) \quad (4.2)$$

Under the dominance of BCS-singularly the matrix element $M^2(\xi_F,\lambda_L,l,\hbar\omega)$ containing momentum $\mathbf{p_i} - \mathbf{p_f} = \mathbf{k}$ and energy conservation $\mathbf{p_i^2} - \mathbf{p_f^2} = \sqrt{(\varepsilon+\hbar\omega)} - \Delta^2 - \sqrt{\varepsilon} - \Delta^2$, Eq. (4.2) can be approximated by [12]

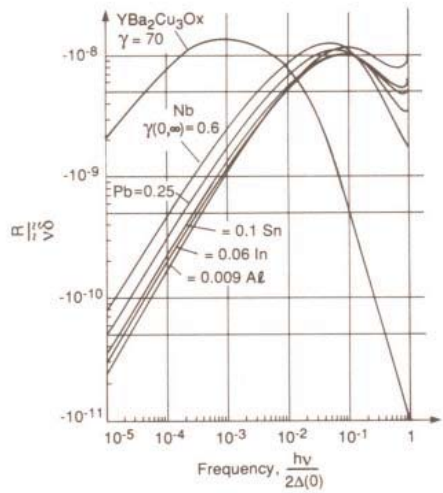


**Fig. 5:** The normalized BCS surface resistance ($R/\nu\delta \propto R/X$) for $T/T_c = 0.2$ and $l \to \infty$ as a function of the reduced frequency $\hbar\omega/2\Delta$ for a number of materials with different values of $\gamma = 2\lambda_L(0)/\pi\xi_0$. The surface resistance is in units of $\Omega$, the frequency $\nu$ in units of GHz, and the London penetration depth $\delta$ is in units of 10 nm.

$$R_{BCS}/\omega\lambda_L \propto \frac{\hbar\omega\exp(-\Delta/kT)}{\sqrt{\Delta\hbar\omega}\,kT} \int dq\,\gamma\left(\frac{\lambda_L}{\gamma^2q^2+1}\right)^2 \mathrm{Re}\sqrt{\frac{\hbar\omega/2\Delta}{\sqrt{\left[\hbar\omega/2\Delta - i\xi_F/l\right]^2+q^2}}} \quad (4.3)$$

yielding for $\gamma \ge 1$ $R/\omega\lambda \propto \gamma$. The mean free path dependence for Nb is shown in Fig. 6, and like Fig. 5, with changes in clear contradistinction to two fluid models, i.e. $R_{BCS}(T)$ decreases ($l > \xi_F$) with enhanced scattering whereas $\lambda(T)$ increases according to Eq. (3).

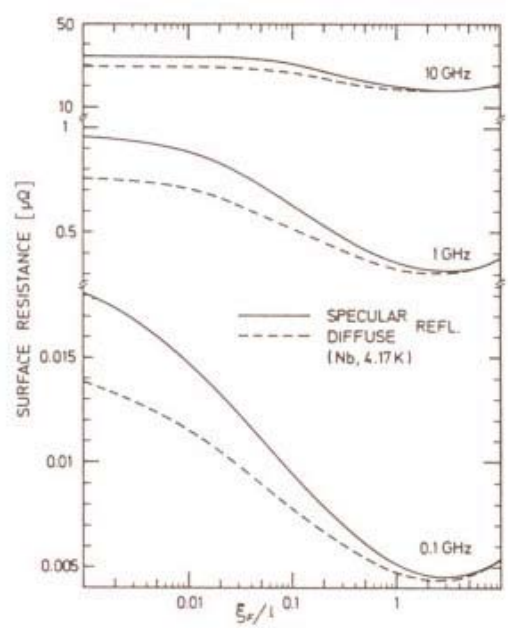


**Fig. 6:** Dependence of surface resistance of Nb (T = 4.17 K) on mean free path l for f = 0.01, 1 and 10 GHz.

### *3.4 Nonlinearities of homogeneous Nb*

Intrinsic nonlinearities, like R-increases due to heating, can be cast in a power series [10a, 13]

$$R(T,f,H) = R(T,f,\approx 10mT)\left[1+\gamma_T^*(H/0.2T)^2+....\right] \quad (5.1)$$

where for Nb as scaling field $H_c(0) \approx 0.2$ T is used substituting $H_c(T)$. For intrinsic nonlinearities $\gamma^*_{BCS} < 0.2$ is estimated as upper limit [13], whereas heating yields larger $\gamma^*_T$ values.

$$\gamma_T^* = \Delta T/\partial R(T)/\partial T/R(T_o) = (R^H(T,H^{\|}) + R^E(T,E^{\perp}))H_c^2/2\cdot\Delta/kT_o\left[\sum\frac{d_i}{\kappa_i}+R_K(T)\right] \quad (5.2)$$

Here $d_i$ and $\kappa_i$ are thickness and thermal resistance of Nb, then for sputtered Nb/Cu the interface resistance has to be added and, at least, the Kapitza resistance $R_K(T)$ toward the He-bath has to be overcome. The heat transfer by phonons is given by their scattering at quasiparticles and phonons which in Nb RRR > 100 is with $l_{ph}(T<4K,<4GHz) \approx 2.6$cm [14] very scarce and, hence, yields for homogeneous, thin (≤ 5 mm) Nb walls ballistic heat transfer from the rf interaction volume to the $Nb/Nb_2O_{5-y}/OH/H_2O$-He-interface. The grain boundaries scatter phonons and in the quasi-amorphous Nb-Cu sputter transition layers $l_{ph} \ll \mu m$ and $\kappa < 0.1$ W/cm K holds [14], yielding $\gamma^* \geq 20$ [10a]. But always the Kapitza resistance has to be overcome, with $\gamma^*(T) \geq 0.3$ increasing below 2 K < $T_\lambda$ = 2.17 K [15].

### *3.5 Inhomogeneous Nb*

Whereas microscopic cluster of, e.g., Ta of 10 µm size, act by their own, weak superconducting properties, small $NbO_x(x < 0.1)$ cluster of sizes below 5 nm < $\xi_F$ show only a slightly depressed order parameter $\Delta^* < \Delta_o$ by depressed superconductivity compensated in part by proximity to bulk Nb, whereas their strain onto the surrounding enhances $\Delta^* > \Delta_o$. Those $NbO_x$-cluster broaden the BCS square root singularity to $\delta\Delta^*$ yielding a reduction of $R_{BCS}$ in Eqs. (4.2 and 4.3) and Fig. 8 to

$$R^*_{BCS}(T,f) \propto (\hbar\omega)^2\exp(-\Delta/kT)/\sqrt{\Delta_o\delta\Delta^*}\,kT$$
$$< R_{BCS}(T,f) \propto (\hbar\omega)^{3/2}\exp(-\Delta/kT)/kT;\ (\hbar\omega \leq \delta\Delta^*) \quad (4.4)$$

Clearly, those cluster reduce also the mean free path l, which by inelastic surface scattering at $n_L$-sites of $Nb_2O_{5-y}$ is already reduced to $l_s \approx 3\lambda_L$. At $NbO_x/Nb_2O_{5-y}$ interface layer the energy transferred to quasiparticles is effectively transferred to phonons via localized states $n_L$. This is different to $NbO_x$-cluster depicted in Fig. 1, where quasiparticles are weakly localized by $\Delta^* < \Delta_o$ with an electron-phonon coupling like in bulk Nb at this temperature. This electron phonon coupling is weak as shown by the inelastic scattering time for $\hbar\omega \ll \Delta$ excitations

$$\tau_{in} \approx 1.15\cdot 10^{-10}(T_c/T)^3\,\text{sec} \quad (6.1)$$

where for T < 4.2 K the recombination time of two quasi particles is negligible. This has to be compared to the quasi particle absorption rate $\tau_{qp}$ [14]

$$\frac{1}{\tau_{qp}} = \frac{B^2_{rf}}{\hbar 2\cdot\mu_o}\,\frac{1}{n_c\hbar\omega}\cdot\frac{R}{X} \quad (6.2)$$

where for Nb with $n_m = 6.3\cdot 10^{22}$/eVcm$^3$ as density of states, $\hbar\omega \approx 10^{-5}$ eV, $B_{rf} \approx 1$mT and $X/R \approx 200$ $\tau_{ab} \approx 10^{-8}$ sec is obtained comparable to $\tau_{in}$. For $B_{rf} > 1$ mT this bottleneck enhances the local temperature T* > T at $NbO_x$-clusters and, thus, according to Eq. (4.2) by $[f(\varepsilon)-f(\varepsilon+\hbar\omega)] \propto \exp(-\Delta^*/kT^*)$, the absorption is reduced. In contrast, adjacent Nb with the mean energy gap Δ, with the absorption given by $\exp(-\Delta/kT)$, easily dissipate the absorbed quanta somewhere in the Nb-wall because of $\tau_{in}v_F \approx 2$ mm, in $\Delta^* < \Delta$-regions confined states overheat by $1/\tau_{qp} > 1/\tau_{in}$ holding locally. This overheating of regions with enhanced rf losses proportional to $\exp(-\Delta^*/kT)$ decreases toward $\exp(-\Delta^*/kT^*)$ by overheating. where according to Fig. 9 and [16]

$$R^*H^2_{rf} \approx \text{const};\quad H > H_{max} \approx \hbar\omega/v_F 3\lambda^H \quad (6.3)$$

holds for energy independent $\tau_{in}$, $R_{BCS}$ is reached above about 10 mT where thermal equilibrium is guarantied because of $v_F\tau_{in} \gg \lambda$ for quasiparticles with energies $|\varepsilon| \geq \Delta$. In line with $\Delta^* \approx \Delta/2$ for $H \leq H_{max}$ in Fig. 9, the BCS-like absorption (Eqs. 4) adds to the $\Delta^*$-region rf losses. Aside of those processes where momentum $\mathbf{p_i} - \mathbf{p_f} = \mathbf{k}$ is transferred to the photon field, the momentum of extended states $|\Delta p| \approx eH_{mas}\cdot v_F 3\lambda^H$ can be transferred to the $\Delta^* < \Delta_o$ localized states, yielding the resonance obvious in Fig. 9 quantified in Eq. (6.3).

### *3.6 Residual rf magnetic losses $R^H_{res}$*

As discussed in [10a] the $Nb_2O_{5-y}$-interface with normal conducting states $n_L(z \geq 0.3$ nm) yields inelastic surface scattering and coherent momentum transfer to the lattice staying finite for $T \rightarrow 0$ with the ITE $\tau(z^*)$ of Eq. (1b)

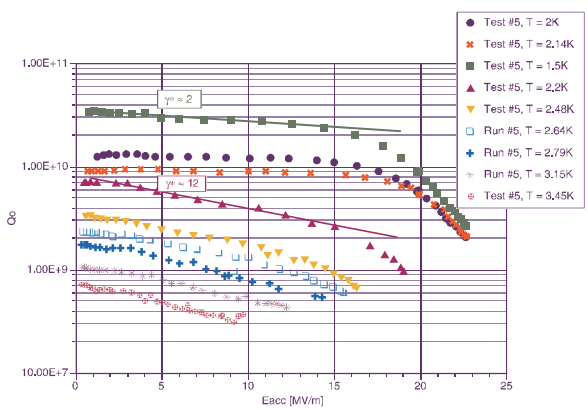


**Fig. 7:** R(T, H)-dependencies of a spun cavity after 150µm chemical polish (BCP) [10]. Obvious is a $\delta 1/Q(H) \propto \gamma^*(H/0.2\ T)^2$ loss increase above 10 mT turning at $E^\circ_{rf}$ to a quasi exponential $\delta 1/Q(E) \propto E^{\perp n}$ (n ≈ 8) increase ending in the breakdown at $R(T,H)\ H^2_{crit} \approx$ const. with a jump at $T_\lambda \approx 2.17$ K. The $\gamma^*(T)$ values show a corresponding jump at $T_\lambda$ from $\gamma^*$ (T ≤ 2 K) ≈ 2 to $\gamma^*$ (T > $T_\lambda$) > 10, whereas the $E^{\perp 8}$-increase is temperature independent – see Sect. 4 and [10a].

$$R_{res}^{In}(T,f) \propto (\lambda^H(T) 2\omega\tau(z^*)) < 5\cdot 10^{-9}\,\Omega (f/GHz)^2 \qquad (7.1)$$

At weak links filled with $Nb_2O_{5-y}$ one has not only reflection but also a normal current in parallel to the Josephson critical current $j_{cJ}$ across the junction (Fig. 1), which yields the Josephson penetration depth $\lambda_J(T,H) \approx \sqrt{\hbar / 2e\mu_o \lambda_L(T) j_{cJ}(T)}$. For weak links in a mean distance $a_J$ with $R_{bl} \propto 1/n_L (\geq 0.3$ nm) as leakage current resistance rf residual losses are obtained.

$$R_{res}^{WL}(T,f) \approx \frac{(2\mu_o \omega \lambda_L(T))^2}{1+(\omega\tau_J(T))^2} \frac{\lambda_J(T)^3}{a_J R_{bl}} \qquad (7.2)$$

$$\text{with } 1/\tau_J = \frac{2e}{\hbar j_{dJ}(T) R_{bl}}$$

as Josephson frequency. For Nb $\lambda^H(T \leq T_c/2) \approx \lambda^H(0)$ and $j_{cJ}(T \leq T_c/2) \approx j_{cJ}(0)$ holds and, hence, below $T_c/2$ the rf residual losses are const. = $R_{res}(T)$.

## 4 EXPERIMENTAL RESULTS

Experimentally, eigenfrequency changes $\Delta f/f_o$ and rf losses, e.g. a decay time, $\tau = Q_o/\omega$ are the observables in rf measurements, being related to the surface impedances by [10,13]:

$$\frac{\Delta\omega}{\omega_o} = \frac{i \oint ds Z^H H^{\parallel 2}}{2\omega_o \mu_o \int dV H^{\parallel 2}} + \frac{\varepsilon_o/\mu_o \oint ds - Z^E E^{\perp 2}}{2i\omega_o \mu_o \int dV H^{\parallel 2}}$$

$$= i\frac{Z^H}{2G^H} + i\frac{Z^E}{2G^E} \text{ for } \left\{H^{\parallel}, E^{\perp}\right\} << \left\{H_c, 10^8 V/m\right\} \qquad (8)$$

For TEM modes $G^H = G^E$ holds, being weakened in TM-modes to $G^H \leq G^E$ approaching $G^E \rightarrow \infty$ for TE-modes. In our analysis of the $TM_{010}$-mode we assume $G^H = G^E$ with $G^H \cong 290\ \Omega$ and peak field ratios $H_p/E_p = 2.5$ mT/MV/m and $E_p/E_{acc} \cong 1.8$

In Figs. 4, 7, 8 and 12 the surface resistances R(T, ≈ 10 mT) ≈ $R_{BCS}(T) + R_{res}$ have been quantified by the BCS theory, resulting in material parameters of Nb in a 40 nm $\approx \lambda^H(T \leq T_c/2)$ surface layers and by $R_{res}(T < T_c/2) \approx$ const, a property of Nb-$Nb_2O_{5-y}$ interfaces, especially weak links. As obvious in Fig. 8 the BCS-theory shows a slower decrease R (f < 10 GHz ) ≈ $f^{1.6}$ than experimental results with oxidized RRR = 30 Nb $R_{exp}(f) \sim f^2$. At 1.5 GHz differences are found between "clean Nb" and UHV-annealed Nb [10], where $R_{BCS}$ decrease by a factor 2 for RRR > 100 Nb and 1.5 for RRR ≈ 30 Nb to the identical lower level. Corresponding to this $R_{BCS}$(10mT)-decrease seems the R(H<10mT)-drop shown in Fig. 9 with an effective gap $\Delta^{**}/kT = \Delta^*/kT^*$ increasing in this direction. For enforced oxidation this drop strengthen (Fig. 10), especially for coldworked Nb. For the same corrosion processes $R_{res}$ is largest for coldworked Nb, see Fig. 8 and [8].

In Figs. 7 and 10 above $E_p \approx 10$ MV/m electric peak field the dependencies are fitted by $\gamma^*(H/H_c)^2$ which depends on T only and not on surface treatment [17-22]. In the Nb cavity with the highest $H_p$ obtained to date, $\gamma^* \approx$ 0.25, $R_{res} \approx 2 \cdot 10^{-9}\ \Omega$ and $H_p \approx 185$ mT > $H_{c1}(1.6\ K) \approx$ 168 mT has been achieved [17]. Hence, $\gamma^*_T(T < T_\lambda) \approx 3$ with $H_p \approx 100$ mT and $\gamma^*_T$ jumping to 12 above $T_\lambda \approx 2.17$ K in Fig. 7 are clearly extrinsic in nature.

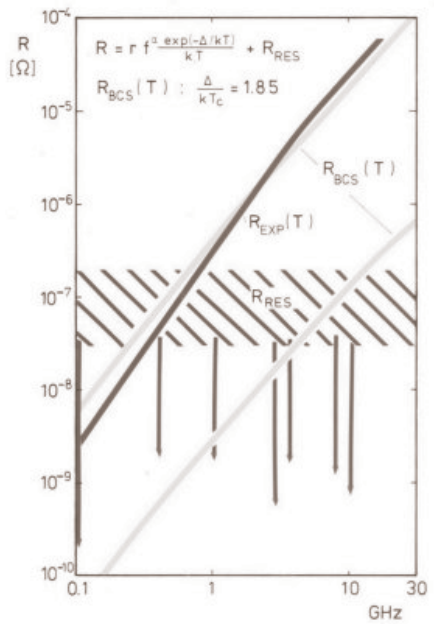


**Fig. 8:** Summary of experimental (RRR = 30) and computed (-) surface resistances of Nb between 0.1 and 30 GHz. The R (4.2 K,f)-values show the cross over of experimental and computed values due to the smearing of the BCS singularity (Eqs. (4.2) and (4.4)). The differences of the computed slopes at 4.2 K and 1.8 K are due to the growth of $\hbar\omega \leq \delta\Delta^* \approx 10^{-2}\ \Delta$. The residual losses show a large scatter depending on surface preparation where cold worked Nb has the highest $R_{res}$-values. The arrows (↓) indicate 1980 best values, which did not improve since then markedly.

Whereas $R^H$ in Eqs. (5.1) are a standard Taylor series, $Z^E$ depends exponentially on $E^\perp$ by tunnel effect for FE and ITE, with a clear onset at $E°_{rf}$ by $z_E \approx \min(z^*(\omega), d_{oxide})$ according to Eqs. (1.2) and (2.2). At this onset an exponential increase sets in which, for experimental analysis, is cast in $R^E(E^\perp) \propto E^{\perp n}$

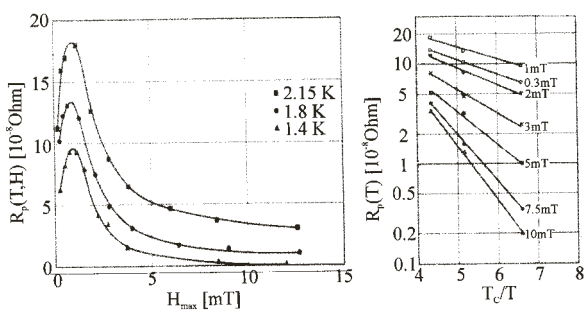


**Fig. 9:** Additional surface resistance $R_p(T,H) = R_{exp}(T,H) - R_{BCS}(T,10\ mT)$ observed at 2.17 GHz in a $TM_{010}$-mode cavity made of RRR = 30 Nb [16]. Above the peak at $H_{max} \approx 1$ mT $R_p(T,H)$ decays like $1/H^2_{rf}$ in (a) where the BCS exponent $\Delta^*/kT^*$ increases toward the mean BCS values shown in (b).

$$\frac{E_{rf}}{R^E}\cdot\frac{dR^E}{dE_{rf}}=\frac{E_{rf}}{R^E}\cdot\frac{2\kappa\Delta}{\beta^* e}\varepsilon_r\left(\frac{1}{E_{rf}}\right)^2\cdot R^E = \frac{2\kappa}{E_{rf}}\frac{\Delta\varepsilon_r}{\beta^*}=n \qquad (9)$$

For the identification of this $R^E$ component

$$R(T,f,H)\approx(R^H_{res}+R^H_{BCS}(T_o,f)+R^E(E^{\perp}))$$

$$(1+\gamma^*_T(H/0.2T)^2+) \qquad (7.3)$$

has to be used, where the geometry factors G weighing in Eq. (8) Z are not correct for non-linear interaction mechanisms, hence local measurements are more appropriate. Those are depicted as temperature maps in Fig. 11, showing no pronounced bad spot but critical $R^E(E^{\perp})$ – heating on a ring with $E\approx E_{crit}$ in this $TM_{010}$-mode, which change by surface smoothening to higher $E_{crit}$ moving closer to the equator where $R^H_{BCS}(T)$ enhanced by $R^E$ via $\Delta T$ yields breakdown on a ring with coarse spots. The smoothing of the rough, spinned surface by successive BCP [18,20] reaches $E_{crit}\approx 30$ MeV/m by successive higher onset fields and higher n-values. Further $E_{crit}$-enhancements need EP yielding $E_{crit}\geq 40$ MeV/m for onset-fields $E°_{rf}\approx 30$ MeV/m in Fig. 13 [22]. The smoothing action on a μm scale by EP has been identified in [23].

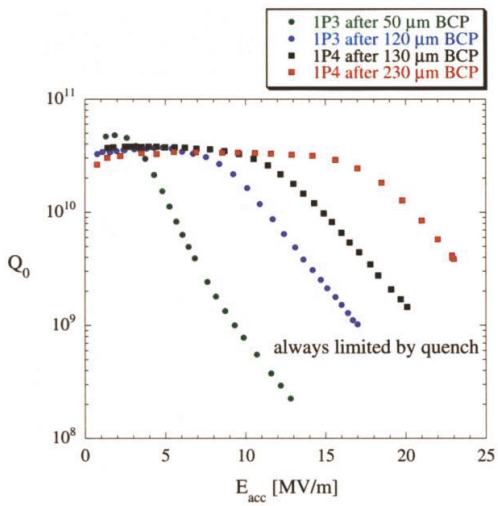


**Fig. 10:** R(2K,H) of a Nb $TM_{010}$-mode cavity at 1.3 GHz spun of RRR ≈ 30 sheath (P2 and P3). The onset fields $E°_{rf}$ = 4.2; 6.3; 13.5; 19.5 MV/m correspond to $E^{\perp n}$ with n = 4; 6; 8; 10 after successive BCP smoothening removing up to 230 μm [18]. Similar changes with BCP-smoothing are reported in [10,21].

## 5 DISCUSSION

The discussion of rf surface resistances starts in Sect. 5.1 with BCS-fits giving Nb material properties in the first 40 nm Nb underneath $NbO_x$. In Sect. 5.2 oxidation and UHV anneal causing inhomogeneities and their non-equilibrium properties are discussed, followed by $R^H_{res}$ in Sect. 5.3. In Sect. 5.4 $R^E$ is analyzed in the light of $Nb_2O_{5-y}$-properties and then in Sect. 5.5 $\delta R^H\propto H^2$.

### *5.1 BCS-Theory and $R_{BCS}(T)$-fits for $H_{rf}\approx 10$mT*

Because of $R_{res}(T\leq T_c/2)=R_{res}$, $R_{BCS}(T\leq T_c/2)$ yields with great accuracy $\Delta/kT_c$ and $R_{BCS}(4.2\text{ K},f)$ as presented in Sect. 3.3 and shown in Fig. 4. In rf cavities for shortest oxidation best $\Delta/kT_c$ values of 1.92 are obtained being still 5 % below clean Nb. This 5 % hints to the standard 3 ML $NbO_x(x\approx 1)$ at the surface and $NbO_x$-cluster depressing locally the gap parameter by more then 30 %. Additional 20 min oxidation yields [8] $\Delta/kT_c\approx 1.84$ – 1.86 by additional O injection and $NbO_x$-precipitation which is enforced by oxidation or 'UHV anneal' at 400 K in excess of 10 h reducing $R_{BCS}$ as found in air anneal already 20 years ago [8] and repeated by Saclay [18]. The reduction starts from $R_{BCS}$-values depending on the initial purity of the Nb after BCP. RRR = 30 Nb has a bulk $l_B\approx 10^2$nm, with $l_S\approx l_B/2$ at the surface and $R_{BCS}(4.2\text{ K})/\mu\Omega$ = 0.8 decreasing to = 0.55 by UHV anneal, whereas RRR ≥ 200 Nb with $R_{BCS}$ (4.2 K)/μΩ = 1 decreases to 0.55 also. Correspondingly, the $\Delta/kT_c$ decreased for RRR ≈ 30 Nb by 3 % and for RRR ≈ 200 up to 1 % only. The $R_{BCS}$ decrease down to 0.55 μΩ for UHV annealed or oxidized Nb cannot be explained by a mean free path reduction of homogeneous Nb, which allows at 1.5 GHz for ideally clean Nb a factor 1.6 or for $l_S\leq 10^2$ nm by ITE a factor 1.2 only as shown in Fig. 6. But smearing the BCS DOS by additional $NbO_x$-precipitates caused by O-in-diffusion and O-precipitation, extending up to 100 – 200 nm deep into the Nb [24] in accordance with O-diffusion into Nb, explains the $R_{BCS}$-reduction up to a factor around 2 at 1.5 GHz with the changed frequency dependence obvious in Fig. 8 and Eq. (4.2). Also the $\Delta/kT_c$-reductions, summarized above, growing with already present defect density down to $\Delta/kT_c\approx 1.7$ are in line with $NbO_x$-precipitates, as has been quantified for RRR = 30 Nb in [8], where the $\Delta/kT_c$-reduction are proportional the BCS DOS smearing inferred by the changed frequency dependence of $R_{BCS}(T,f)$.

### *5.2 UHV-anneal, $NbO_x$-cluster and deviations from thermal equilibrium*

In 100°C UHV anneal $Nb_2O_{5-y}$ becomes thinner on account of O diffusion and $NbO_x(x\ll 1)$ precipitation into Nb. The $Nb_2O_{5-y}$ thinning has been measured by ARXPS [6] and by ITE (Fig. 12 and Sect. 5.5), the $NbO_x$ diffusion depth has been measured by stripping [24] and the O-precipitates by $\Delta/kT_c$-reductions, by $R_{BCS}$-reductions analyzed above and by $R_{res}$ increases discussed in Sect. 5.3. All those degradations are observed also for standard oxidation already - see Sect. 5.1. The finite size of $NbO_x$-cluster localize quasi particles in the $\Delta^*<\Delta_o$ potential, which are easily driven out of thermal equilibrium. This has been worked out in Sect. 3.5 yielding $R_p(H<10\text{ mT})\propto 1/H^2$ as decrease. As shown in Figs. 9,10 and 12 this effect is the more pronounced the more $NbO_x$-cluster are present, as, e.g., for cold worked Nb in Fig. 10 or RRR ≈ 30 Nb in Fig. 9. There, reduced gap values for $H\approx H_{max}$

are obvious also. The peak shown in Figs. 7, 9, 10, 12 and 13 is due to the energy gain transferred to those cluster explained in Eq. (6.3).

### *5.3 Magnetic rf residual losses $R^H_{res}$*

As obvious by Fig. 7, coldworking and enforced oxidation enhances $R_{res} \propto \omega^2$ [25] by enforced weak link growth, discussed in Section 3.5 and [8]. By enforced UHV anneal, e.g., above 150°C or heating Nb in air above about 90°C, $R_{res}$ is systematically growing [8,20-25] in line with Sect. 3.5. $R_{res}(1.5\ GHz) \leq 10^{-8}\Omega$ is dominated by short junctions t < 20 nm and inelastic surface scattering [25c,d] discussed in Sect. 3.5. The short junction depicted in Fig. 1 penetrate into Nb by crack corrosion [5,8] yielding $R_{res}(T<T_c/2, H_p < 1\ T) \approx R_{res}$ [12a,25b].

### *5.4 Dielectric surface resistance $R^E(T,E)$*

Dielectric losses in the insulator coating are an old proposal for rf residual losses quantified by [25a]

$$R^E_{BIEL} = \frac{f}{GHz}\,\frac{d_{diel}}{nm}\,\frac{tg\delta}{\varepsilon_r \cdot 10^{-5}} \cdot 4 \cdot 10^{-11}\,\Omega\,, \qquad (2.3)$$

being much smaller then the observed ones – see Fig. 8. For anodized Nb $R^E_{diel}$ becomes measurable in TM-modes above $10^2$nm $Nb_2O_5$ only, despite all those defects existing in wet or galvanic $Nb_2O_{5-y}$. The dielectric loss mechanism introduced in Sect. 3.2 is a specific interface mechanism making use of the high density of states in metals $n_m$ adjacent to an oxide layer containing localized states $n_L$. Systematic studies on $R^E(T,E)$ are rare because of its smallness, but ITE grows linearly with $n_L(\varepsilon)$ and, hence, $Nb/Nb_2O_5$, $Ta/Ta_2O_5$ and high $T_c$ superconductors (HTS) show the largest effective ITE's [10,12b]. Because $R^E$ and $R^H$ are intermingled - see Sect. 3 - a clear separation of both rf residual losses is not possible. But at high fields $R^H(H)$ follows a Taylor expansion (Eq. (5.1)) being distinctively different from the exponential, tunnel current like increase of $R^E(E^\perp)$ allowing an unique separation of both effects.

In $TM_{010}$-mode Nb cavities at fields $E^\perp_p \geq 10$ MV/m the Q-drop or 'European decease' [17-24] is encountered. That is, an electron loading free, field emission like increase $R^E \propto \exp(-c/E^\perp)$ is observed starting at $E°_{rf}$ with n = 4 – 16 in Figs. 7 and 10 and Sect. 3.1 without $E^{\perp 2}$-, $E^{\perp 4}$- and $E^{\perp 6}$- terms needed for a Taylor series. Most experimental results on $R^E(E^\perp)$ are assembled on spun Nb-cavities [10,18,21,24], where the initial roughness was reduced by BCP and tumbling. In accord with the surface smoothing and removed cold worked surface layer, the onset field $E°_{rf}$ increases from $E°_{rf} \approx 6$ to 36 MV/m with n = 4 to 8 - 16 as exponent in $\delta R^E \propto E^{\perp n}$. For $\Delta^* \approx 1.5$ meV, $\varepsilon_r \approx 15$ and $\kappa \approx 2$/nm at Nb-$Nb_2O_5$ interfaces – see Eqs. 2, Figs. 7 and [10,12b] – this corresponds to $\beta^* \approx 5$; 2 - 1.5 for the static $E^\perp$-field enhancement factor. This fit factor $\beta^*$ is not simply a field enhancement factor but includes also the observation of Fig. 11, that the largest effect

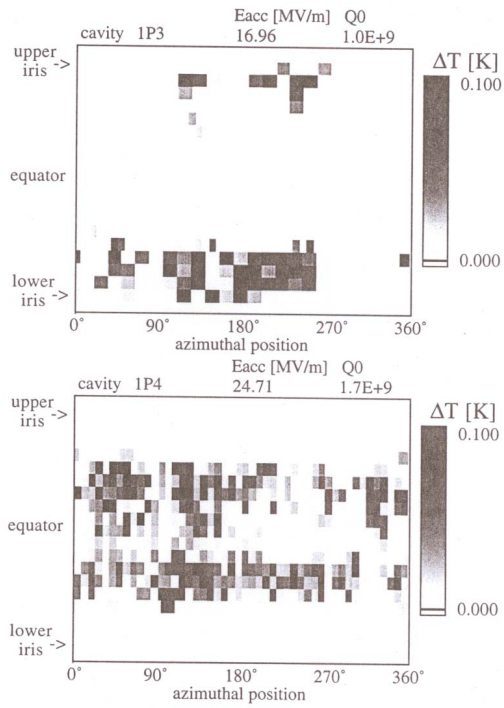


**Fig. 11:** Heat maps at different field levels for spun Nb cavities P3 and P4 of reactor grade Nb (RRR ≈ 30) at fields just below the quench at $H_{crit}$ showing in this field region an $E^\perp$-$Q_o$-drop with $6 \leq n \leq 12$ in Fig. 9. The maximum temperature rise was 0.4 K in order to display also areas with lower heating. The rotational symmetric heatings, which do not show a pronounced spot typical for impurities or stripes for field emission, shifts with increasing $E°_{rf}$ away from $E_{max}$ towards $H_{max}$ enhancing there by heating the temperature dependent losses $R^H(T)H^2$.

occurs at equatorial rings which shifts to smaller $E_p/E_{max}$-values with BCP-smoothing where, in addition, Eq. (7.3) yields via $\Delta T \propto E^{\perp n+2}$ a multiplication by an $R^H H^{n+2}$ increase obvious in Fig. 11b. Further smoothing of the BCP surfaces by EP reduces $R^E(E^\perp)$ with increased $E°_{rf}$ and n values, as obvious in Fig. 13 allowing to reach $E_{acc}$ > 30 MeV regularly [22]. Those values are obtained by UHV anneal after BCP shown in Fig. 12, where $R^E(E) = A\,E^8$ decreased in A by a factor 10.

As proven above, ITE gives a quantitative description of the Q-drop with accepted interface parameters. $R^E$ decreases with smoothening of surfaces by BCP followed by EP [22], in line with the $\beta^* E_p$-dependence in Eqs. (2). The temperature dependencies presented in [10] confirm, that $R^E_{ITE}$ is temperature independent below 3 K, which is in line with Sect. 3.2 and $\Delta^*(T) \approx \Delta^*(0)$ below $T_c/2$. The result of Fig. 12 of $R^E$-reduction by UHV anneal thinning the dielectric $Nb_2O_{5-y}$ layer to thicknesses below 1 nm < $z_E$(35 MeV/m) for most of the surface confirm Sect. 3.2 also.

### *5.5 Magnetic field dependencies $R^H(T,f,H_{rf})$*

If hydrogen is removed properly from the surface layer either by UHV 800°C anneal or by $NbO_x$-precipitates at the Nb surface, the linear $R^H(F,f,H_{rf})$ increase by flux

penetration [9,25d] is absent. Then $R^H_{res}(H<1T) \approx$ const. above $H_{rf} > 10 - 20$ mT holds as overall and consistent description of $R^H(T,H)$ of Nb cavities fabricated from Nb sheeth. As uppermost limit for intrinsic BCS nonlinearities $\gamma^* < 0.2$ is estimated. Clearly, Figs. 7 and 10 with $\gamma^*_T(T) \geq 1$ are extrinsic and due to heating as the temperature dependence of $\gamma^*_T(T)$, especially the jump at $\lambda \approx 2.17$ K, proves. This and the ballistic phonon heat transfer through 0.3 cm Nb due to a phonon mean free path $l_{ph} \approx 2$ cm for $T < T_c/4$ hints to the phonon escape via the $Nb/Nb_2O_5$ interface (Fig. 1) into the He as bottle neck, i.e. to an enlarged Kapitza resistance $R_K \approx 1$ cm$^2$ W/(T/K)$^4$ [15]. As given by Eq. (5.2) $\gamma^*_T(T_o) \propto R_{BCS}(T_o)/T^2_o$ increases for $T > T_\lambda$, whereas below $T_\lambda$ the Kapitza resistance $R_k \propto 1/T^4$ overcompensates the $R_{BCS}(T)/T^2$ dependence in Eq. (5.2) yielding the observed $\gamma^*(T)$ increase below 2 K in Fig. 7. At $E^\perp$ fields where $R^E$ becomes comparable to $R_{BCS}(T)$ locally the $R^E$ induced heating $\Delta T$ gets multiplied exponentially by $R_{BCS}(T + \Delta T)$ yielding the heat map and breakdown at rings in small distance to the equator in Fig. 11b, which in their grainy structure reflect ITE governed by the local field enhancement factors $\beta^*$.

The exchange rate $1/\tau(z)$ of Eq. (1.1) has to be faster than 1/2f to yield ITE as one-hop up to distances of 1.5 nm along the shear planes in Fig. 2. Consequently ITE is more pronounced at 0.1 GHz then at 1.5 GHz. Shear planes ending at $NbO_x$ ($x \leq 1$) seem to be less frequent in the smoother, dry oxides yielding a smaller a $E^n$ term than in wet oxides. Because ITE is confined to a interface layer at forthcoming changes of the outer surface (Fig. 1) by oxide growth or water and hydrocarbo chemisorption will change ITE negligibly only. This is in contrast to electron loading depending on those outer layers, as discussed in [7,26].

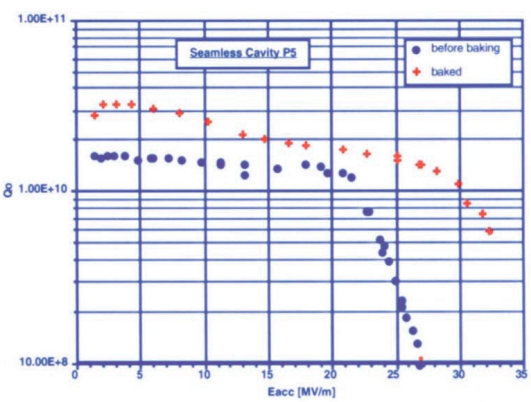


**Fig. 12:** UHV anneal for 40 h at 145°C of the spun Nb (P5; RRR ≈ 250) cavity after 100 μm BCP reducing the $E^{\perp 8}$ term. Worth mentioning is the deepened R(H)-minimum below 5 MeV/m by baking and the reduced $E^{\perp 8}$-term by a factor 10.

### *5.6 RF-breakdown*

The above analysis of Nb cavities of superior quality, i.e. no local degradations of superconductivity, e.g. by Ta- or Fe-cluster, enhancing $R^H$ or no dust or no electron loading enhancing $R^E$, show that for bulk Nb the heat transfer at the Nb-$Nb_2O_5$-He interface and $R^E(E^\perp) \propto \exp(-c/E^\perp)$ defines the nonlinearities and the rf breakdown roughly with $H^2_{crit}\, R(H_{crit}) \approx$ const. for $T < T_\lambda$. For the best cavity with $E_{crit} = 44$ MeV/m and $H_p \approx 0.19$ T > $H_{c1}(1.6K) = 0.168$T [17]. In this cavity, the critical heat load $[R^E(E_{crit}) + R^H(H_{crit})]\, H^2_{crit}/2$ is a factor of about 2.5 larger after 2 years, where $E_{crit} = 27$ MeV/m have been reached only, with an indication of $R^E$. In the spun cavities the critical heat load below $T_\lambda$ is more than a factor 5 higher then for the 44 MeV/m BCP cavity and in those cases the $R^E$-term yields a grainy heating on rings close to the equator – see Fig. 11 – for $E_{acc} > 20$ MeV/m becoming more grainy for $E_{crit} < 15$ MeV/m on rings close to the iris. Those very grainy appearances below $E_{crit} < 15$ MeV/m become unstable at critical heat flows being a factor 25 higher than for $E_{crit} \approx 44$ MeV/m, hinting to the fact, that ITE by local field enhancements causes high losses locally, stabilized by the surrounding, especially by the lateral heat flow caused by $R_K$. This stabilization grows for $T > T_\lambda$ by the higher boundary resistance [15] even more, as shown by critical heat flows jumping at $T > T_\lambda$ by factors larger than 2. This will not happen for $H_p$ aproaching $H_{sh}$ where the surface properties and heating are more uniform and, hence, the critical heat flux lower.

What is the reason for the rf breakdown? Not talking about extrinsic but intrinsic causes only, line nucleation yield in [27a] for clean Nb the critical superheating field $H_{sh} \approx 0.2$ T. Close to $H_{sh}$ also the penetration depth $\lambda$ increases with H [27b] yielding in $R_{BCS}(H)$ higher powers in $H^{2n}$, intrinsically not to be discussed here. Because near the surface local defects ($NbO_x$ . . . – see above) causes a mean gap reduction of 10 % or more, line nucleation may be eased averaging over $2\xi_F > 100$ nm Nb, which may correspond to the observed 5 % $H_{sh}$ reduction [17a]. The above mentioned small ($\ll \xi_F$) defects by themselves will not cause breakdown because their deteriorated $\Delta^*$ values by up to 30 – 50 % are stabilized by proximity and deviation from thermal equilibrium discussed above.

## 6 SUMMARY AND CONCLUSION

As shown in the above analysis the present state of Nb surface preparation yields dielectric $Nb_2O_{5-y}$ layers of thicknesses above 2.5 (wet) or 1.5 nm (dry) containing more (wet) or less (dry) shear planes per surface area with localized states $n_L \leq 10^{19}$/cm$^3$. The enhanced $Nb_2O_{5-y}$ or $NbO_x$ ($x \leq 1$)-volume compared to Nb creates $Nb_2O_{5-y}$ weak links and $NbO_x$ cluster, depending on Nb quality or oxidation process. Those surface deteriorations act on high $Q_o$ Nb cavities at high fields ( > 10 MeV/m) mainly by ITE between the $n_L(z \leq 1.5$ nm) states and the conduction electrons of the metallic $NbO_x$ surface causing $R^E \propto \exp(-c/E^\perp)$ and inelastic surface scattering. The local electric field $E^\perp$ is reduced by surface smoothing by BCP, being enforced by EP, where the $n_L$-density is reduced by

UHV anneal, in addition.

The $\Delta/kT_c$ reduction compared to bulk Nb in the standard, oxidized Nb surface layer (≈ 40 nm) by 10 % to about 1.84 by $NbO_x$-layers and –cluster enhances $R_{BCS}(T)$ which is reduced by BCS-density of states smearing, being enhanced by mild (< 150°C) UHV anneal. The 10 % gap reduction may yield some $H_{sh}$-reduction but because of the $\xi_F \approx 60$ nm stabilization this reduction is smaller than 10 %. The reduction may be avoided by an NbN-surface layer with $T_c \approx 15$ K being more corrosion resistant avoiding $NbO_x$-cluster in Nb and wet-oxides on $Nb_2O_{5-y}$ [8]. The Kapitza resistance $R_k \propto T^{-4}$ for present day RRR > 100 Nb dominates the heating enhancing rf losses causing finally rf breakdown, favoring working temperatures around 2 K.

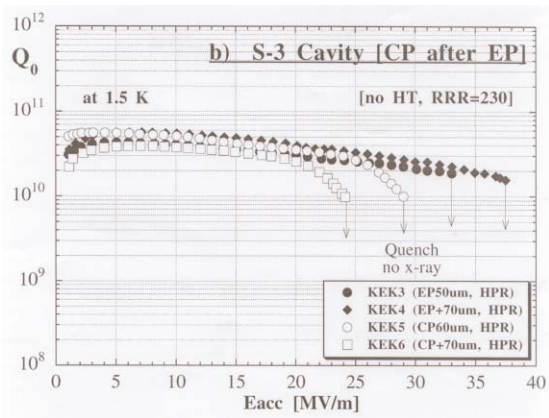


**Fig. 13:** Cavity degradation due to BCP after EP by a $Q_o$-drop signaling growing $R^E \propto \exp(-c/E^{\perp})$ losses [22].

## ACKNOWLEDGMENT

Many thanks are due to A. Dacca, P. Kneisel, L. Lilje, K. Saito and B. Visentin for their interesting and intense discussions. The author thanks KEK, especially S. Noguchi and K. Saito, for the support making the presentation and this paper possible.

## REFERENCES

[1] H. A. Schwettman et al., Adv. Cryogenic Engineering, Vol. 10 (K. Timmerhaus Ed., Plenum Press, 1965), p. 88 and Proc. IV Int. Conf. on High Energy Acc., Stanford 1974 (SLAC 1974), p. 123

[2] A. Citron et al., KfK-report 3/76-5 and KfK 3019 (Kernforschungszentrum Karlsruhe)

[3] Proc. First [second, third, . . . tenth] workshop on rf superconductivity, Karlsruhe, 1980; [Cern, 1984; ANL, 1987; Los Alamos, 1999; Tsukuba 2001]

[4] P. Kneisel in [3] and J. Vac. Sci. Technol A 11, 1575, (1993)

[5] M. Grundner, PhD-thesis (Uni Karlsruhe, 1977) and J. Appl. Phys. 51, 397 (1980)

[6] A. Dacca, PhD-thesis (INFN and Uni, Genova, 2000) and Appl. Surf. Science 126, 219 (1998)

[7] J. Halbritter IEEE Trans EI-18, 283 (1983) and EI-20, 671 (1985), and Appl. Phys. A 39, 49 (1986)

[8] J. Halbritter, J. Less Common Metals 139, 133 (1988) and Appl. Phys. A 43, 1 (1987)

[9] J. Halbritter et al., Proc. 6 Workshop on rf superconductivity CEBAF, 1997, p. 617

[10] J. Halbritter, Proc. 38 Eloisatron Workshop, Erice, Oct. 99 (World Science Publ. 2000), p. 59
b) J. Halbritter, IEEE Trans Appl. Superconductivity 11, 1864 (2001) and references therein

[11] Vu Thien Binh et al., Phys. Rev. Lett. 85, 864 (2000) and J. Vac. Sci. Technol. B 18, 956 (2000)

[12] a) J. Halbritter, Z. Phys. 266, 209 (1974) and J. Superconductivity 4, 341 (1991)
b) J. Halbritter, Z. Phys. B 31, 19 (1978)

[13] a) J. Halbritter, J. Appl. Phys. 41, 4581 (1970)
b) J. Halbritter, J. Superconductivity 8, 691 (1995)

[14] J. Halbritter, Primärbericht 08.02.02 P06B (IKP, FZK, 1979) and to be published

[15] M. Mittag, Cryogenics 13, 94 (1973); J. Amrit et al., Proc. CEC-01, Madison, July 2001.

[16] P. Kneisel et al., Low Temperature Physics – LT13, Vol. 3 (Eds. K. D. Timmerhaus et al., Plenum Press, N. Y. 1974), p. 202

[17] P. Kneisel, Proc. 7. Workshop on rf superconductivity, Oct. 1995, Gif sur Yvette (IN2P3, 1996) p. 449 and Proc. 8. workshop on rf superconductivity, Abano Terme, Oct. 1997 (V. Palmieri, A. Lombardi, Eds.; LNL-INFN-Rep. 133, 1898), p. 463

[18] M.Pekeler, ibid, p. 820

[19] K. Saito et al., ibid p. 795

[20] B. Visentin et al. ibid, p. 198 and Proc. 6th EPAC, Stockholm, July, 1998, p. 1885

[21] a) P. Kneisel et al., Part. Acc. Conf. (1999) and IEEE Trans Appl. Supercond. 9, 1023 (1999)
b) P. Kneisel, Proc. 9 workshop on Rf superconductivity, Los Alamos, Oct. 99, p. 446

[22] K. Saito et al., ibid, p. 179 and 288

[23] C. Antoine et al., ibid p. 295

[24] P. Kneisel, ibid. p. 328

[25] a) J. Halbritter, Proc, 2 Workshop on rf Superconductivity, Geneva, 1984 (CERN report, 1984), p. 427
b) M. Regier et al., IEEE Trans Appl. Superconductivity 9, 2375 (1999)
c) J. Halbritter Supercond. Science and Technology 12, 883 (1999),
d) J. Halbritter, J. Appl. Phys. 68, 6315 (1990) and 71, 339 (1992) and J. Superconductivity 8, 691 (1995)

[26] M. Grundner, J. Halbritter, J. Appl. Phys. 51, 5396 (1980)

[27] a) T. Yogi, PhD thesis (CalTech, 1976)
b) H. Parr et al., Phys. Rev. B14, 2842 (1976) and B19, 3482 (1979)